3
Ni-based Enzymeless and Transparent Glucose Sensor

(Cited work: Urgunde et al., ACS Appl. Nano Mater. 2018, 1, 5571−5580)

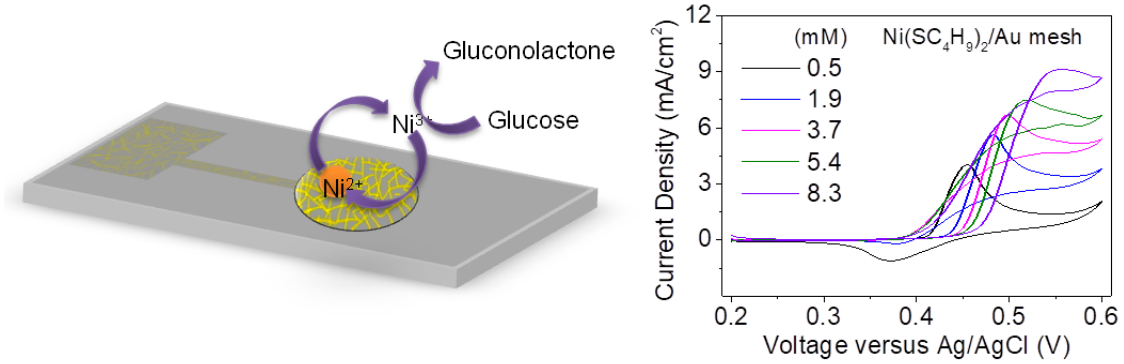

3.1 Introduction

Diabetic patients have to go through rigorous medical checkups to control the advancement of the disease.[Golrokh Amin et al., 2019] The blood glucose monitoring of the patients helps prevent diabetic emergencies like hypoglycemia or hyperglycemia to avoid prolonged complications that can cause kidney failure, blindness, and high blood pressure etc. The advancements in glucose-sensing devices are desirable to a highly sensitive and accurate glucose measuring system (Figure 3.1). If diabetic patients are given such convenient, low cost and durable shelf life glucose sensors, it is more likely to measure the glucose levels very often with regular intervals, which will allow them to optimize their insulin injections and medications.[Chandrasekaran et al., 2020]

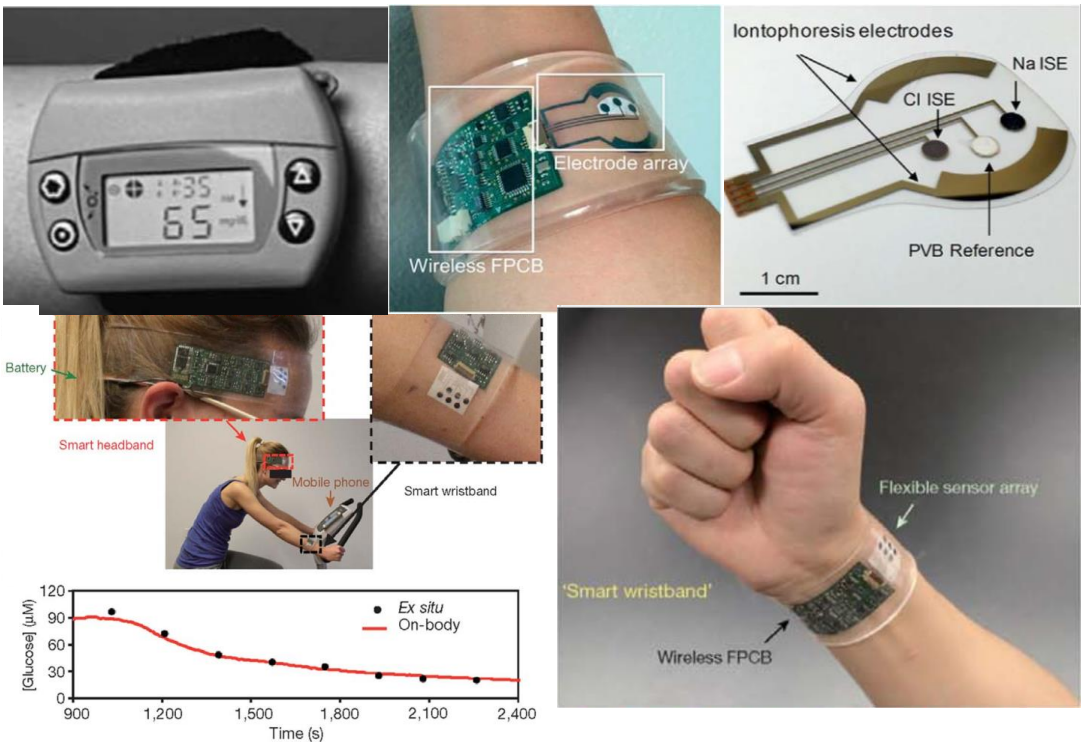

Figure 3.1: Flexible sensors for glucose detection. Figures adapted from reference [Kim et al., 2018a].

Ni/NiO-based nanostructures are excellent materials for the fabrication of glucose sensors. However, none of the sensors reported are transparent. Further, there is a dire need to develop easily scalable production methods for the commercialization of these glucose sensors. Most of the literature methods are based on non-scalable synthetic techniques and thus, not yet commercialized. Ni alkanethiolate-based precursors in toluene can be easily prepared as ink for direct application by a solution-based process. Moreover, thiolate ink is known to bind well with metallic substrates such as Au and Ag. In this chapter , a series of Ni alkanethiolate are synthesized as single-source precursors, and electrodes are fabricated by drop-casting these on conducting substrate. It is further electro-oxidized, resulting in a thin electrocatalytic layer for electrochemical glucose sensing. This method has the advantage of obtaining well-distributed redox-active centers without any aggregation resulting in reproducible and stable results. Among different chain length thiolates, Ni butanethiolate with a short alkane chain results in high current density at lower voltage and acts as an optimum coating for sensing application. The transparent Au mesh showed high electrochemical sensing performance for non-enzymatic detection of glucose due to the high electrocatalytic activity of Ni butanethiolate.

3.2 Objectives of the Work

The objectives of this work are as follows:

1. To fabricate Ni-based electrodes using Ni alkanethiolates with varying chain length as functional ink.
2. To optimize the fabrication process for the development of patterned Au mesh by toner transfer technique.
3. To study the electrochemical properties of fabricated electrodes for glucose sensing for wide range of detection.

3.3 Experimental

3.3.1 Materials and Synthesis

The Ni-BT precursor was synthesized using general two-step process, detailed in Chapter 2, Section 2.4.2. In a similar way alkane thiols (RSH; R= C_4H_9, C_8H_{17}, $C_{12}H_{25}$, and $C_{16}H_{33}$) were used for the synthesis of Ni octanethiolate, Ni dodecanethiolate, Ni hexadecanethiolate. The obtained Ni alkanethiolates were solubilized in toluene to make 1 mg/mL of solution for electrode fabrication.

3.3.2 Fabrication of Plain Au Electrode

The Au film and fluorine-doped tin oxide (FTO) (Product Code-TISXZ001, Techinstro substrates, sheet resistance 7 Ω/sq) working electrodes of 3 mm diameter were fabricated by patterning toner masking technique developed in this study followed by Au metal evaporation. Crackle lithography was employed for the fabrication of Au mesh electrodes as detailed below. Different Ni alkanethiolates complex solutions (5 µL) in toluene were drop coated and allowed to dry for 2 hr before use.

3.3.3 Fabrication of Au Mesh and FTO based Electrodes

The Au mesh was prepared by the crack template method. Briefly, a commercially-available crackle finish paint (DecoArt, USA) is mixed with IPA and water at 80:20 to a concentration of 0.5 mg/mL, sonicated for 10 min spin-coated on glass substrates at 800 rpm for 30 s. Upon drying, the coated layer forms a network of well-connected cracks. The Au metal is deposited

by physical vapor deposition (PVD) in the active area of 5 mm diameter using a physical mask, and the crack template is removed by dissolving in chloroform, leaving behind Au network on a glass substrate. The patterned substrates were examined using an Optical Microscope (Laben, India). The physical mask of the toner was first printed on a PET sheet and transferred to the glass substrate by hot pressing the toner printed side of PET towards the glass substrate at an optimum temperature of 200˚C. The FTO and Au films were patterned by physical masking created using a hot press toner transfer technique on standard FTO and glass substrates.

3.3.4 Material and Device Characterization

The absorbance spectra were recorded using a UV-Vis spectrophotometer (Varian Cary 4000) over a 200-800 nm wavelength range. Fourier Transform Infrared spectroscopy (FTIR) was performed using Bruker Vertex 70 V+ PMA50 spectrometer in the range of 600 to 3000 cm^{-1}. The sample preparation was done by pelletizing the complex with standard KBr (analytical grade). FESEM measurements were performed Nova NanoSEM600 instrument (FEI., The Netherlands). XPS characterization was carried out on Omicron Nanotechnology (Oxford Instruments). Samples for XPS were prepared by drop-coating Ni thiolate on Au/glass substrates.
Electrochemical measurements were performed using an electrochemical workstation (CHI660E-CH Instruments Inc.). The cyclic voltammetry (CV) was done in three-electrode geometry with Ni alkanethiolate coated Au metal network, FTO and Au film as working electrodes, Ag/AgCl as the reference electrode, and Pt as the counter electrode. NaOH (0.1 M) was used as an electrolyte. A voltage range of 0.2 - 0.8 V was chosen, and measurements were performed at different scan rates (10 - 350 mV/s). Glucose solution was made in 0.1 M NaOH. Electrochemical measurements were carried out with various electrodes in different concentrations of glucose solution. The CV measurements of blank Au electrode were carried out in 0.1 M blank NaOH at a scan rate of 50 mV/s as control. The reproducibility of the glucose sensor was examined by testing five different electrodes under the same conditions as described in the experimental section.

3.4 Results and Discussion

3.4.1 Characterization and Fabrication of Ni-BT Functionalized Au Electrode

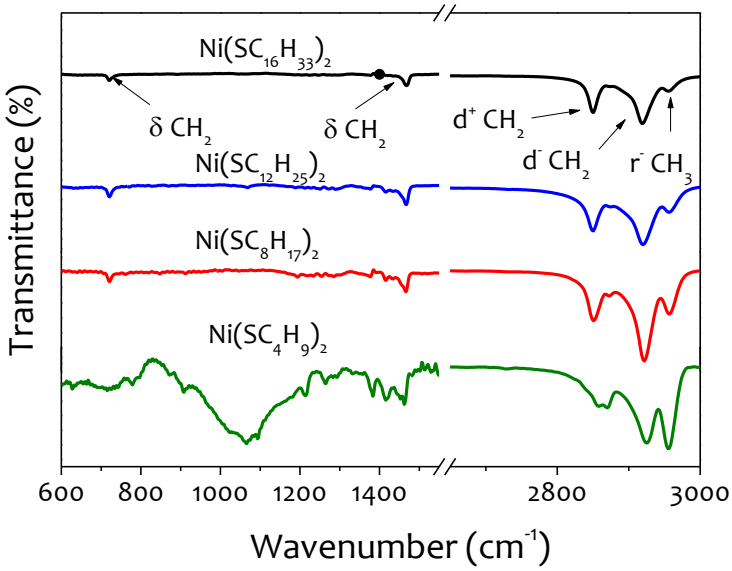

Figure 3.2: Characterization of Ni alkanethiolate of different chain lengths by FTIR spectroscopy. (b) UV-visible spectroscopy.

The Ni alkanethiolate complexes of different chain lengths were synthesized following the procedure as explained in the experimental section.[Gupta et al., 2017a; John et al., 2007b] Briefly, solution of nickel chloride and alkanethiol were mixed in the presence of triethylamine in ethanol at 70°C with vigorous stirring resulting in a precipitate due to complex formation. All the complexes were characterized by FTIR and UV-vis spectroscopy, as shown in Figures 3.3. In FTIR spectra, all the peaks are indexed, as shown in Figure 3.2 and 3.3. With the increasing chain length, there is an apparent increase in peak intensity of anti-symmetric CH_2 peak. In the UV-vis spectra (Figure 3.3), all the signatures are ascribed to ligand to metal charge transfer, and since there is no peak corresponding to d-d transition for tetrahedral Ni(II), it suggests a square planar arrangement of Ni(II).

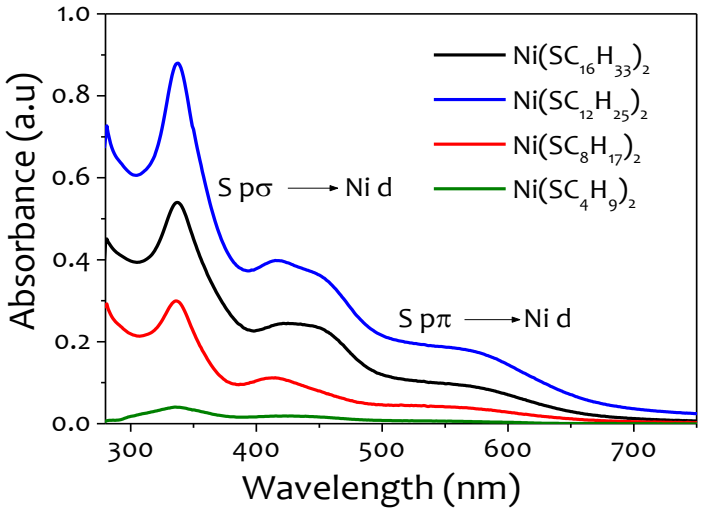

Figure 3.3: Characterization of Ni alkanethiolate of different chain lengths by UV-visible spectroscopy.

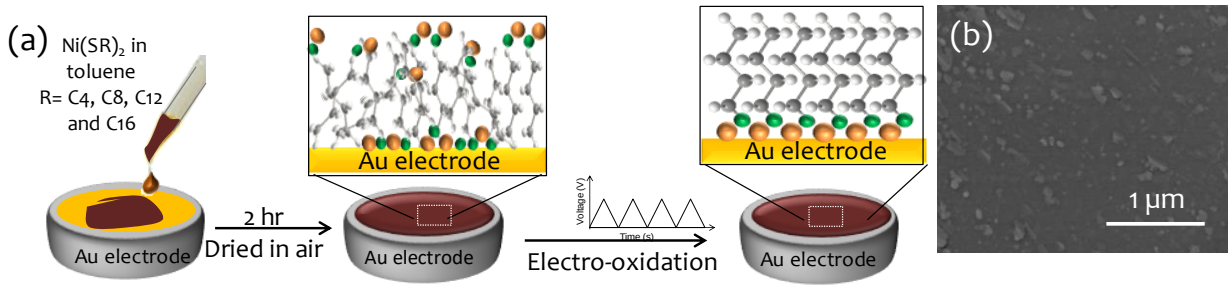

Figure 3.4: (a) Fabrication of working electrode for electrochemical measurements. (b) FESEM image of the electrode after electro-oxidation.

These complexes are dissolved in toluene and drop-coated on Au film, as shown by the schematic in Figure 3.4. The Ni alkanethiolate complexes on drop coating form a uniform thin film on the electrode surface despite the random orientation of molecules due to the lamellar structure of these complexes.[Rao et al., 2011a] The Ni alkanethiolates molecules on the Au electrode are subjected to consecutive cyclic voltammetry cycles for electrooxidation of the Ni alkanethiolate chains leading to self-assembly of molecules under applied field (Figure 3.4a). The FESEM image in Figure 3.4b shows the well-distributed random nanoparticles present on the electrode surface after electro-oxidation. The CV cycles are repeated until a saturated voltage, and current is obtained, as shown in Figure 3.5a. The Ni(II) thiolates redox is observed to be quasi-irreversible and the repeated CV cycling helps in the ligand exchange reaction. Thus, CV cycles are carried out till a constant current state is attained inferring complete conversion of the surface to $Ni(OH)_2$. The term electrooxidation is used to indicate the surface

activation process through consecutive CV cycles. The CV was also performed with different scan rates as shown in Figure 3.5b to ensure the absence of redox peaks in the voltage window of interest.

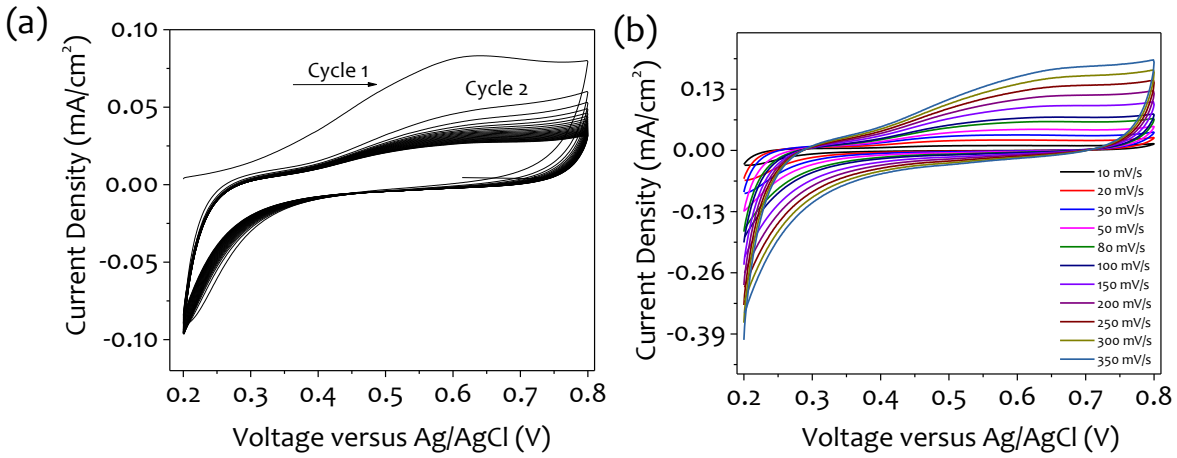

Figure 3.5: CV measurements of blank Au film in 0.1 M NaOH (a) for 25 cycles at 50 mV/s and (b) with increasing scan rates.

The first voltammetric curve represents the oxidation of the Ni ions to $Ni(OH)_2$ in 0.1 M NaOH (indicated by the first cycle with different peak potential). Since blank Au electrode did not exhibit any peak around 0.4 - 0.6 V in CV measurement (Figure 3.6a), the redox peaks correspond to Ni alkanethiolates only. This is also the reason for selecting Au as the current collecting electrode. The progressive increase in anodic and cathodic peak currents can be seen with the oxidation of $Ni(OH)_2$ to NiOOH.[Sivakumar et al., 2016; Yu et al., 2012] As seen in Figure 3.6a, the repeated measurements increase current density and peak shifting towards lower potential values. The highest anodic peak current was observed in $Ni(SC_4H_9)_2$/Au (henceforth abbreviated as Ni-BT/Au) with the current density of 1.06 mA/cm², whereas Ni-C16SH/Au exhibits the lowest current density of 0.12 mA/cm² even after 25 cycles. The increase in current could be due to the reorientation of molecular ligands during redox activity.[Karikalan et al., 2016]

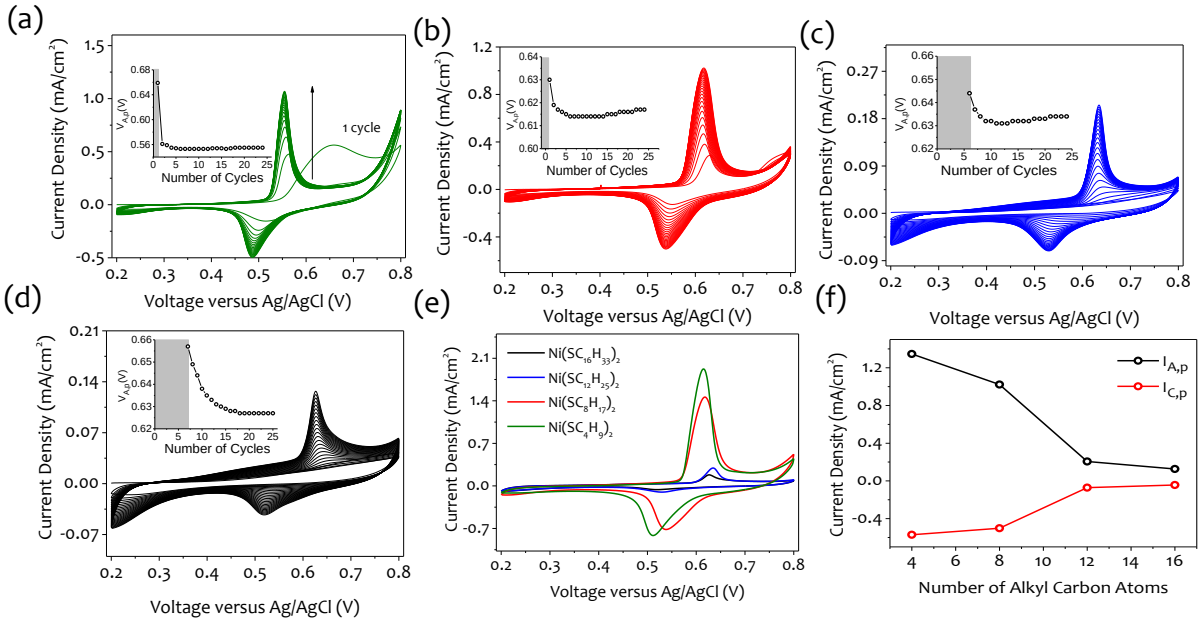

Figure 3.6: CV scans for the first consecutive 25 cycles for Ni alkanethiolates, $Ni(SR)_2$, where R = (a) C_4H_9, (b) C_8H_{17}, (c) $C_{12}H_{25}$ and (d) $C_{16}H_{33}$ respectively in 0.1 M NaOH solution. Insets in each section show corresponding peak voltage variations with respect to the number of cycles. (e) Electrochemical behavior of $Ni(SR)_2$ complexes (R= C_4H_9, C_8H_{17}, $C_{12}H_{25}$, and $C_{16}H_{33}$) at 50 mV/s after electro-oxidation step. (f) Anodic and cathodic peak current density with respect to the number of carbon atoms in the $Ni(SR)_2$.

Moreover, Ni-BT possesses distorted structure compared to other long-chain thiols where ordering is lamellar.[John et al., 2007b] The measurements were continued for 25 cycles till the saturated current was obtained along with a constant peak potential. This process helps eliminate the ligands on the surface and exposes the Ni redox-active centers directly to the electrolyte. The anodic peak current for the thiolates increases with respect to descending carbon chain length (I_{C4}>I_{C8}>I_{C12}>I_{C16}). The peak shift is much more drastic from 0.70 V to 0.55 V in the case of Ni-BT/Au as compared to other longer chain thiolates (inset, Figure 3.6a). In the case of Ni-C8SH/Au and Ni-C12SH/Au, the peak shift occurs only after several cycles (inset Figure 3.6b and c), while in case of Ni-C16SH/Au in Figure 3.6d, the redox peak is absent in the beginning and takes several odd cycles for a low current peak (31.97 µA) to originate at 0.65 V. Moreover, the peak in first cycle has different potential than that of the rest of the cycles. The insets of the Figure 3.6a-d represent the anodic peak potential ($V_{A,p}$) values of the respective thiolates. After the pre-electrooxidation, it is observed that with the number of cycles, the peak potential stabilizes to a particular potential with the oxidation of $Ni(OH)_2$ to NiOOH.[Chen et al., 2016; Mu et al., 2011] The stability in the peak potential for the initial 25 cycles can be seen from the insets of Figure 3.6a-d. From Figure 3.6e, it can be seen that the peak position of the Ni alkanethiolates changes with the increasing number of carbon atoms. An increase in anodic peak current with an increasing number of alkane carbon atoms is shown in Figure 3.6f. A steep decrease in anodic peak current is observed with an increasing number of alkane carbon atoms. Peaks are shifting more towards the positive side with an increased peak current due to higher electron hopping resitance offered by the longer alkane carbon chain.[Wuelfing et al., 2002] As the carbon chain length increases the ion diffusion rate is limited and thus more potential is required for the electron transfer; hence a change in peak position towards the positive side is observed. Similarly, with the decrease in the carbon chain, the number of electrons hoping through increases, leading to an increase in current at a much lower peak potential which is essential for electrochemical activity. The butane chains in Ni butanethiolate are known to be defective and attains various conformations that may result in highly exposed Ni(II) redox centers.[John et al., 2007b] This leads to higher redox activity within the same area than the other Ni-based alkanethiolates.

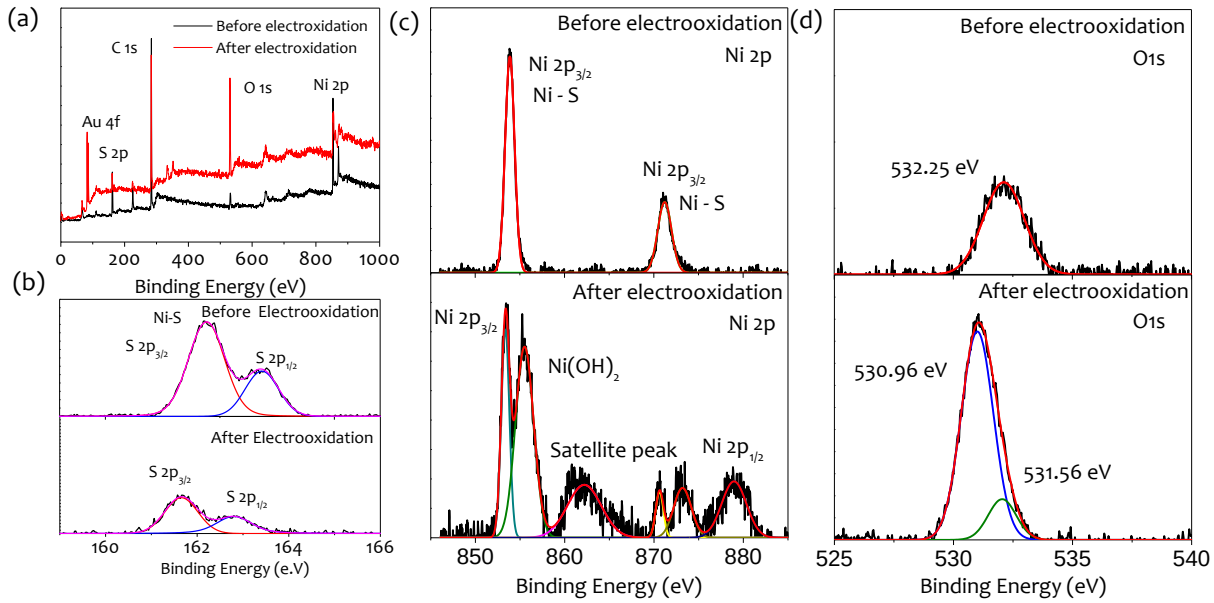

Figure 3.7: Survey spectra (a) High Resolution XPS spectra of (b) S 2p, (c) Ni 2p and (d) O 1s in Ni-BT/Au electrode before and after electro-oxidation.

The detailed surface composition and oxidation were carried out by X-ray photoelectron spectroscopy (XPS) on the Ni-BT/Au electrode before and after electrooxidation by applying 100 cycles of CV at 50 mV/s. The full survey spectra show the presence of peaks corresponding to Ni 2p, O 1s, S 2p, Au 4f, and C 1s, as seen in Figure 3.7a. After electrooxidation, there is a shift

in Ni(II) peaks to lower binding energy (853.6 eV and 870.64 eV) due to the weakening of Ni-S linkage and emergence of new peaks at 855.6 eV and 873.2 eV corresponding to $Ni(OH)_2$ formation (Figure 3.7b).[Karikalan et al., 2016] In the high-resolution spectrum of the Ni 2p regime, two peaks were observed at 853.8 eV and 871.04 eV corresponding to Ni $2p_{3/2}$ and Ni $2p_{1/2}$ due to the Ni(II) species in the thiolate complex Figure 3.7c. The spin energy separation of ~17 eV is attributed to the formation of $Ni(OH)_2$. A satellite peak is as well observed at 861.16 eV. To further confirm the presence $Ni(OH)_2$, high-resolution O 1s spectra were deconvoluted as seen in Figure 3.7d. For the pristine electrode, a small peak was observed at 532.5 eV, which corresponds to the M-O bond due to surface oxygen species. On electrooxidation, two highly intense peaks appear at 530.9 eV and 531.5 eV, corresponding to the oxide species along with surface hydroxylation.

3.4.2 Electrochemical Measurements

The Ni-BT/Au was used further for testing the electrochemical performance towards glucose sensing. The electrochemical sensing properties of Ni-BT/Au were investigated using cyclic voltammetry in the presence and absence of 1 mM glucose solution in 0.1 M NaOH at different scan rates as shown in Figure 3.8. The redox peaks obtained for Ni-BT/Au in blank NaOH and 1 mM glucose are shown in black and red color curves, respectively (Figure 3.8a and b). The well-defined redox peaks at 0.50 V (cathodic peak) and at 0.55 V (anodic peak) in Figure 3.8a-d correspond to Ni^{2+}/Ni^{3+} redox couple formation with an increase in scan rate. However, for the same scan rate, an apparent increase in current is observed upon adding 1 mM glucose to the blank NaOH solution. The slight shift in peak potential and increased current is observed with successively increasing scan rate, as shown in Figure 3.8a-d.[Zeng et al., 2016]

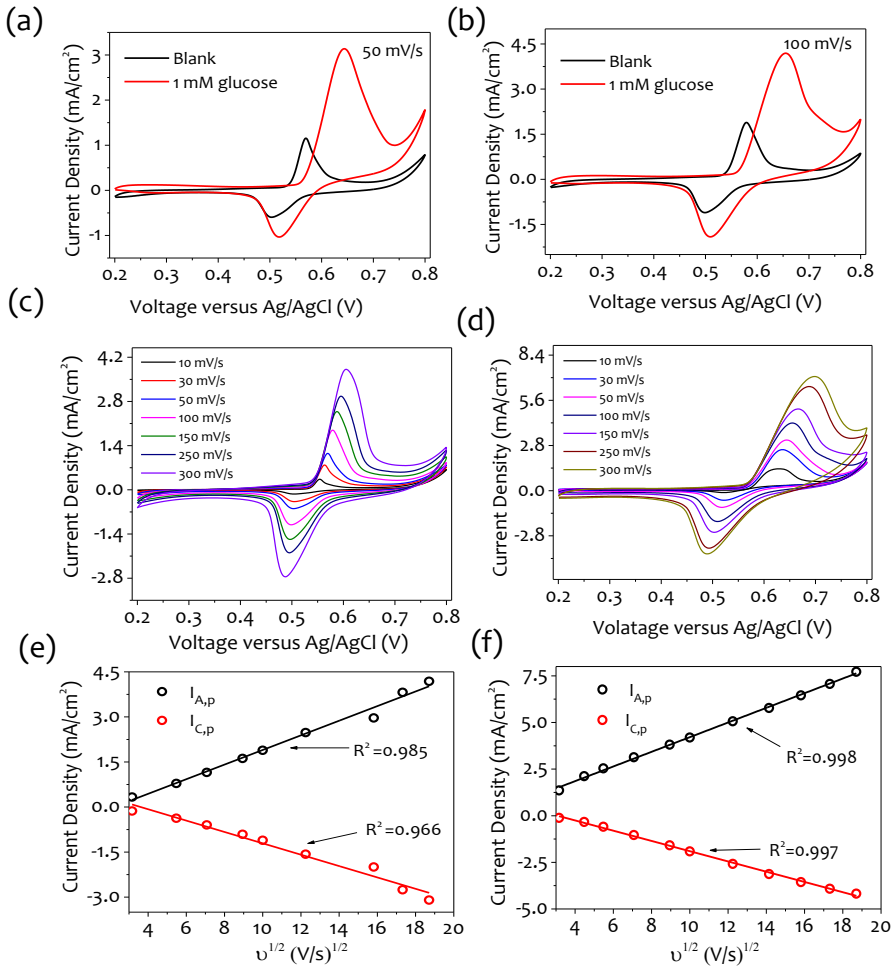

Figure 3.8: Electrochemical properties of Ni-BT/Au as a working electrode. (a and b) CV scans of Ni-BT/Au with and without glucose (1 mM) at different scan rates of 50 and 100 mV/s respectively (c and d) without and with 1

mM glucose (scan rates 10 – 300 mV/s). The relation between anodic and cathodic peak current with respect to scan rates (e) in 0.1 M NaOH (f) 1 mM glucose.

The plausible reason is because of the oxidation of glucose to gluconolactone by NiO(OH) accompanied by the formation of $Ni(OH)_2$.[Manikandan et al., 2016; Wang et al., 2016c] Figure 3.8e and f demonstrate the linearity of anodic and cathodic peak current ($I_{A,p}$ and $I_{C,p}$) the square root of different scan rates for blank and 1 mM glucose, respectively. It can be seen that $I_{A,p}$ and $I_{C,p}$ both increase linearly with the increasing scan rate. The linear relationship in both cases is important for the sensing device as it indicates the reversibility of the electron transfer process taking place during the electrochemical reaction. The correlation coefficient, $R^2 = 0.998$ in Figure 3.8f confirms that Ni nanostructures formed by the electro-oxidation of Ni butanethiolate possess excellent electrocatalytic activity for enzymeless glucose oxidation. The above results in Figure 3.8 show that Ni nanostructures derived from Ni-BT layer is electrocatalytic active towards glucose sensing.

3.4.3 Fabrication of Au Mesh Electrodes

The Au mesh electrodes were fabricated by a combination of toner transfer patterning and crackle lithography, as shown schematically in Figure 3.9a. The crackle precursor spontaneously cracks, resulting in an interconnected network of empty space that is filled with Au metal by physical vapor deposition in a masked region. The physical masking is done by transferring laser jet printed toner on a PET sheet to a glass substrate by hot pressing, as demonstrated in Figure 3.9a. The resulting Au network possesses a sheet resistance of Au mesh is ~ 4 Ω /sq, which is slightly higher than the Au film ~ 2 Ω/sq.

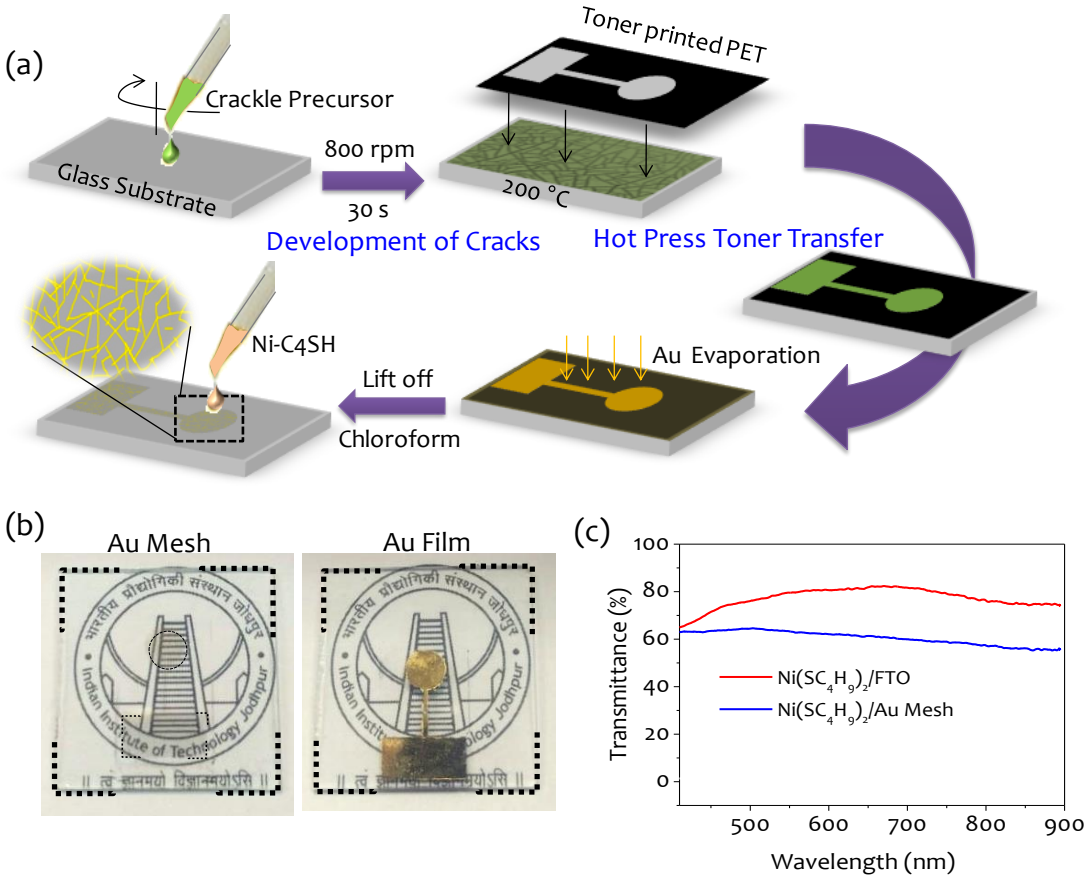

Figure 3.9: (a) Fabrication of Au mesh functionalized with Ni-BT (b) Photographs of Au film and Au metal mesh electrodes. The letters below the electrode are clearly visible through the mesh network. (c) The transmittance spectra of $Ni(SR)_2$ coated on Au film, FTO and Au mesh based electrodes.

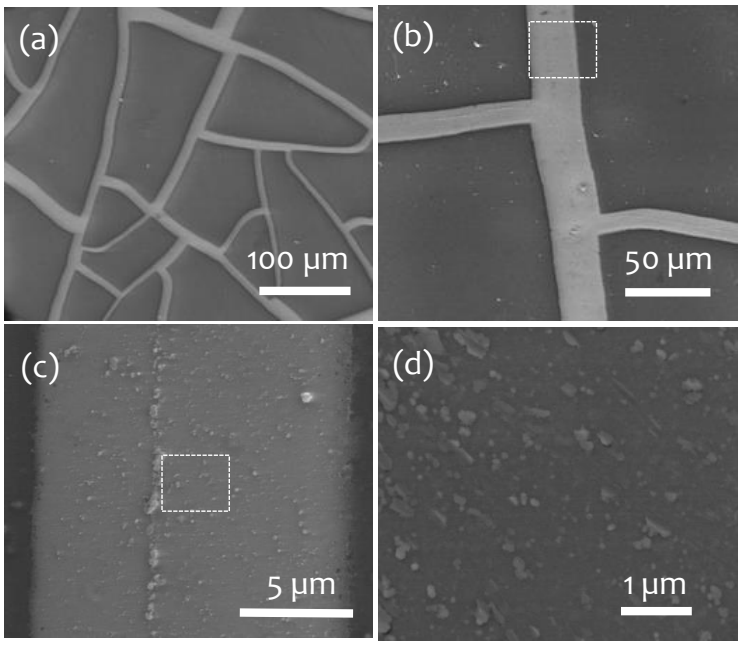

Figure 3.10 (a-d) FESEM images of the crack network at different magnifications.

However, it appears to be significantly transparent (Figure 3.9b). The transmittance of Au mesh coated with Ni-BT was measured to be ~ 60 % which is slightly lower than Ni-BT/FTO; however sufficient enough for clear visibility (Figure 3.9c).

The transparency of metal mesh is attributed to the voids present between the seamlessly connected wire networks (Figure 3.10) fabricated by crackle lithography technique.[Rao et al., 2014] The electrochemical behavior of the electrode is further examined for their application as functional material in glucose sensors. Au film and Au mesh electrodes were functionalized with Ni-BT layer and electro-oxidized as described before to understand if there are any differences in their electrochemical response with and without glucose due to changes in the electrode geometry.

3.4.4 Glucose Sensing Performance of Au plain and Au Mesh Electrodes

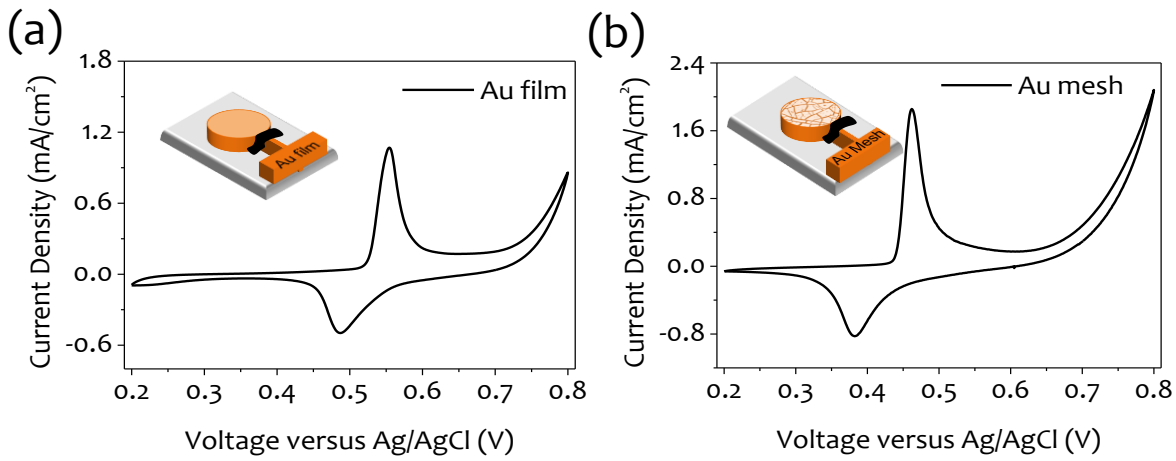

Figure 3.11: (a and b) CV measurements of Ni-BT/Au film and Ni-BT/Au mesh as working electrodes at a scan rate of 50 mV/s .

CV curves of Ni-BT/Au film and Ni-BT/Au mesh after electro-oxidation in 0.1 M NaOH are shown in Figure 3.11a and b. The oxidation peak corresponding to Ni^{2+} is obtained at much lower potential using Au mesh electrode as compared to the Au film. However, the reversibility of Ni-based redox reaction is lowered for Au mesh as indicated by the higher peak-peak

separation as well as the ratio of peak currents. Clearly, Au mesh-based electrodes can enable sensing at lower operating voltage due to low oxidation potentials in contrast to Au film.

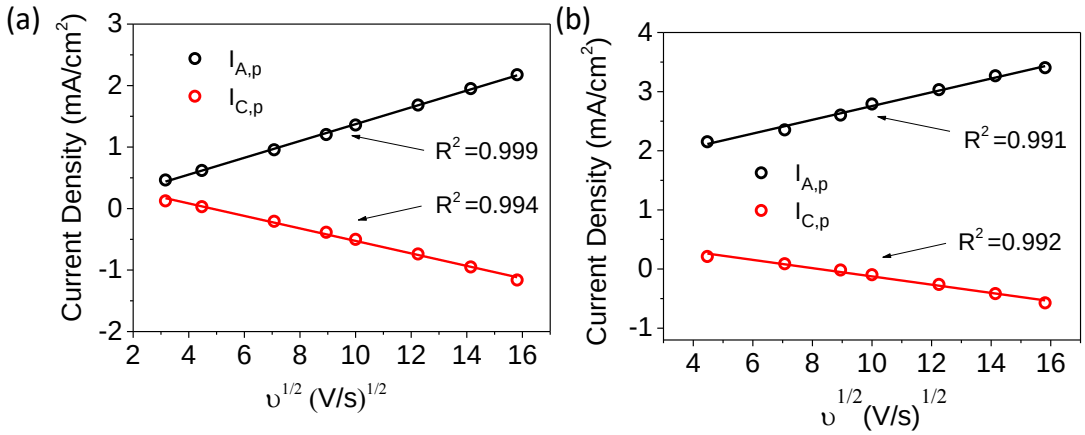

Figure 3.12: Relationship between peak current and scan rate for Au mesh electrodes (a) in 0.1 M (Blank) NaOH (b) 1 mM glucose solution.

For understanding the glucose response, CV curves were obtained in the range of 0.2 - 0.8 V versus Ag/AgCl for Au film and 0.2 - 0.6 V versus Ag/AgCl for Au mesh . The current density is observed to be linear with respect to square root of scan rate for Ni-BT/Au mesh electrode with and without glucose as shown in Figure 3.12a and b indicating the catalytic activity of Ni based electrode is not compromised by using modified Au mesh electrodes as well.

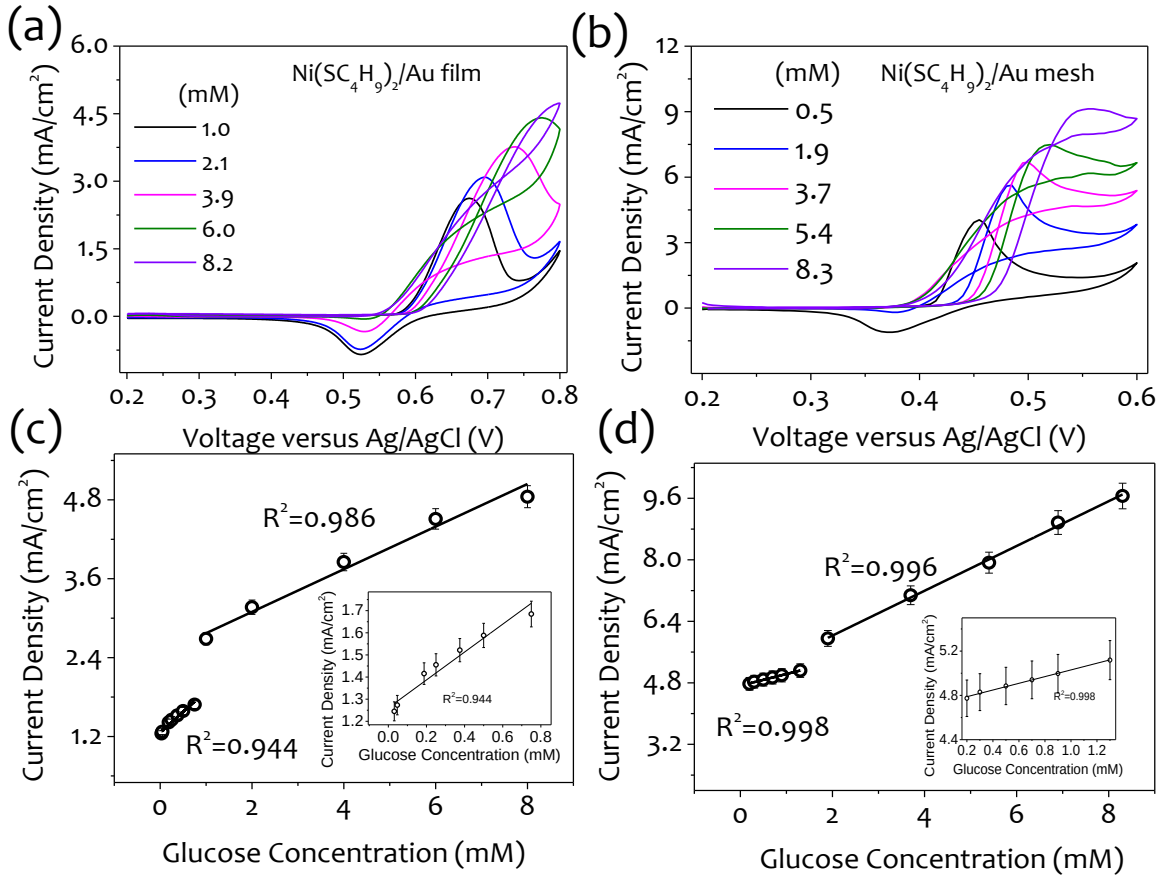

Figure 3.13: (a-b) CV measurements for different glucose concentrations and the calibration plots (c-d) of Ni-BT/Au film and Ni-BT/Au mesh respectively.

A constant increase in the anodic peak current and decrease in cathodic peak current is seen with the increasing glucose concentrations in both the cases (seen in Figure 3.13a and b) in

accordance with the literature. [El-Nagar et al., 2017; Liu et al., 2018c; Rajendran et al., 2018] However, the onset potential and the voltage range for electrocatalytic activity is different for Au mesh and Au film. The Au mesh is made of a seamless wire network that offers a high surface area to glucose molecules and reduces the overpotential for oxidation to ($V_{p,mesh}$ = 0.45 V) in comparison to Au film ($V_{p,\ film}$ = 0.55 V). The electrocatalytic activity in Au mesh is relatively more pronounced in reverse cathodic scan at positive potentials as seen by the raised current with respect to that of Au film based electrode. The reversibility of the mesh based electrode in presence of high concentration of glucose (< 4 mM) is relatively low, however sufficient enough for one-time glucose sensing application. The highest anodic peak current of the CV curves of Au film and Au mesh for each glucose concentration is plotted and fitted linearly to obtain two different ranges of concentration. The higher region was observed from 1 - 8 mM for Au film and 2 - 8 mM for Au mesh. The lower ranges lie between 0.03 - 1 mM and 0.2 - 1.5 mM for Au film and Au mesh respectively. The glucose concentration versus current density obtained from anodic peak current values display an excellent linearity with a correlation coefficient value, R^2 = 0.944 and R^2 = 0.998 of glucose concentration below 1 mM and 1.5 mM in case of Ni-BT/Au film, and Ni-BT/Au mesh respectively (Figure 3.13 c and d). Similarly, for the higher region, the R^2 values were 0.986 and 0.996.

Table 3.1: Comparison in performance parameters of the $Ni(SC_4H_9)_2$ functionalized Au film, Au mesh and FTO electrodes obtained from CV measurements.

S. No.	$Ni(SC_4H_9)_2$/ Electrode	R^2 value	Linear Range (mM)	Sensitivity μA/(mM cm^2) (slope)	LOD (μM) (Calculated) = 3σ/slope
1	Au film	0.944	0.03 - 1	590	0.799
2	Au film	0.986	1 - 8	131.32	20.082
3	Au mesh	0.998	0.2 - 1.5	272	1.746
4	Au mesh	0.996	2 - 8	549	7.610
5	FTO	0.971	0.5 - 5.5	303.66	2.563

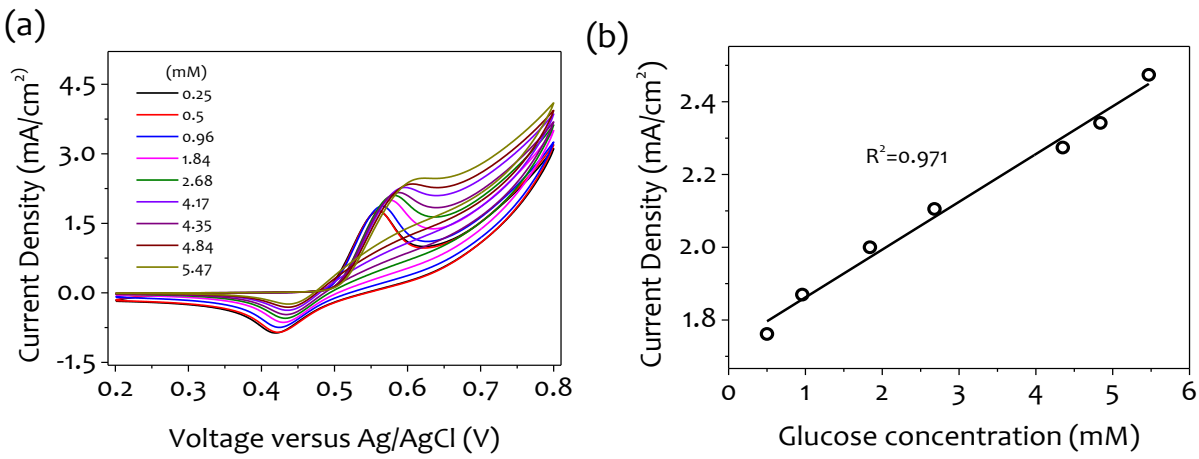

Figure 3.14: CV measurements of $Ni(SC_4H_9)_2$/FTO at (a) different glucose concentrations (2.5- 4.8 mM) and its corresponding (b) calibration plot obtained from anodic peak current at each glucose concentration.

The results obtained with transparent Au mesh electrode are comparable with Au film electrode. However, FTO electrode possess a very narrow range of detection (0.5 - 5.5 mM) and R^2 = 0.971 indicating lower electrocatalytic activity of Ni-BT/FTO towards glucose oxidation probably due to lesser electron conduction compared to Au (Figure 3.14). The performance metrics of different electrodes are compared in Table 3.1. The value of sensitivity and LOD is

calculated. The value of R^2 for Au mesh specifically indicates high electrocatalytic activity with high sensitivity in lower ranges of glucose.

To further study the performance of the Ni-BT/Au mesh and $Ni(SC_4H_9)_2$/FTO electrodes as sensors, I-t measurements were performed for both the electrodes in three-electrode geometry at an applied voltage of 0.6 V as shown in Figure 3.15a and b respectively. Systematic jumps in the current are observed with time in an otherwise constant current density at 0.6 V upon successive addition of aliquots of 50 mM glucose in 10 mL of 0.1 M NaOH. In case of Au mesh, it takes more time to respond to the glucose as compare to that of FTO. This may be due to lower 2-D surface area of the wire electrode thus giving a time delay in the current response. The glucose is added to the system until no change in current is observed. A saturation limit is obtained after glucose concentration becomes 11 mM for Au mesh and 5.3 mM, in case FTO electrode suggesting faster coverage of actives sites on FTO surface by intermediates formed during reaction making them less available for incoming glucose molecules as compared to Au mesh.

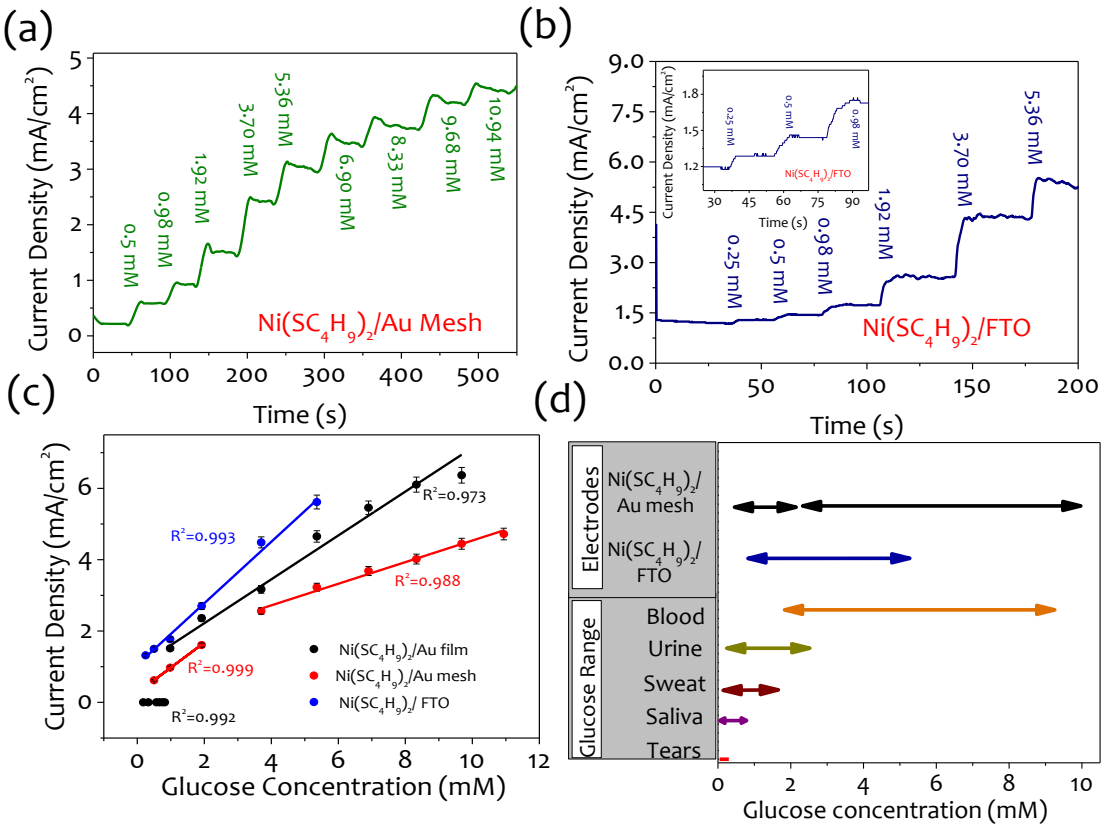

Figure 3.15: Sensitivity and Specificity towards glucose detection (a) Amperometric response of (a) Ni-BT/Au mesh and (b) Ni-BT/FTO at 0.6 V towards the successive addition of glucose of different concentrations in 0.1 M NaOH. (c) Calibration plot for different concentration of glucose for Au film, Au mesh and FTO electrode. (d) Glucose detection range for the transparent Au mesh and FTO compared with different analytes/ body fluids available for glucose detection.

Clearly, the projected surface area of Au mesh that is electrochemically active is comparatively higher than FTO due to the lateral contribution from the thickness of the wire network even though the geometrical area of metal mesh is lower (25%). It is important to note that the concentration range of detection is wider for Au mesh as compared to FTO and human blood glucose range lies between 1- 8 mM that makes Au mesh based electrode ideal for glucose sensing. The calibration plot obtained from the i-t measurement in Figure 3.15c shows two different concentration regimes where the current response is linear. The R^2 value is 0.999 in lower concentration region of 0.5 - 2 mM with and 0.988 for Au mesh in the higher region of 2 - 11 mM. These values are comparatively better than that of FTO and Au film based electrodes (Figure 3.15c).

Table 3.2: Comparison in performance parameters of the $Ni(SC_4H_9)_2$ functionalized Au film, Au mesh and FTO electrodes obtained from I-t measurements.

S.No.	$Ni(SC_4H_9)_2$/ Electrode	R^2 value	Linear Range (mM)	Sensitivity μA/(mM cm^2)	LOD (μM) (Calculated) = 3σ/slope
1	Au film	0.992	0.18 - 1	171.12	0.737
2	Au film	0.973	1 - 9.68	564.7	11.827
3	Au mesh	0.999	0.5 - 2	675.97	2.167
4	Au mesh	0.988	2 - 11	325.74	7.170
5	FTO	0.993	0.25 - 5.5	852.05	6.082

The sensitivity and LOD were found to be 675.97 μA.$mM^{-1}cm^{-2}$ and 2.167 μM (S/N = 3) for Au mesh for lower region. The Ni-BT/FTO electrode exhibited the sensitivity of 852.05 μA.$mM^{-1}cm^{-2}$ and a LOD of 6.082 μM (S/N = 3) as obtained from the slope and extrapolation of linear calibration curve of I-t measurements, respectively (Table 3.2). The wide range of glucose detection in Au mesh can be attributed to the interconnected 2D-wire network with high electrode/electrolyte interface that provides more active sites to the glucose molecules. Figure 3.15d shows the actual range of values of glucose present in body fluids such as urine, saliva, and sweat. The higher range of detection was experimentally observed to be 2 - 11 mM for Ni-BT/Au mesh electrode which can be easily used for detecting blood glucose simultaneously the lower range of detection is from 0.5 - 2 mM and which can be used for a variety of body fluids. For Au mesh, glucose detection range is wider as compared to FTO and thus it can be used for the blood glucose detection as well. Interference tests were also performed with other molecules that might be present in low quantities in blood (0.1 mM) along with higher concentrations of glucose (3 - 8 mM).

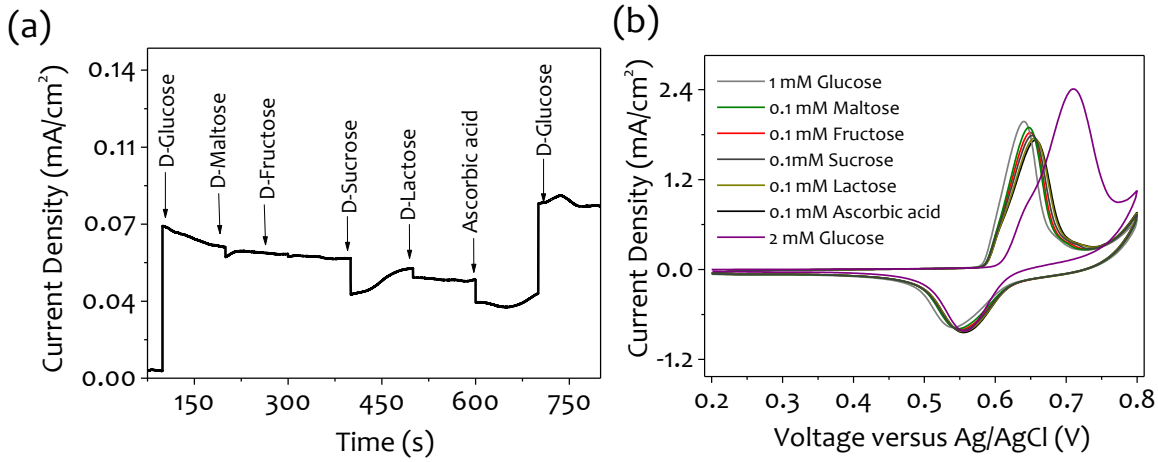

Figure 3.16: (a) I-t measurement and (b) CV measurements of $Ni(SC_4H_9)_2$/Au film for sequential addition of interfering molecules of 0.1 mM concentration to 1 mM glucose in 0.1 M NaOH. No signification change is observed in the peak potential. This is followed by addition of 2 mM of glucose resulting in a anodic peak shift to 0.73 V versus Ag/AgCl.

I-t and CV measurements were performed with the successive addition of glucose and other interfering sugars such as 0.1 mM maltose, 0.1 mM fructose, 0.1 mM sucrose, 0.1 mM lactose and 0.1 mM of ascorbic acid with Ni-BT/Au electrode (Figure 3.16a and b). Since, the other molecules are usually present in much lower concentrations compared to the concentration of the glucose in blood sample; we have used 0.1 mM concentration of the interfering molecules. The change in the current density is observed to be marginal as compared to the change in the

current density upon exposure to 1 mM concentration of glucose. After addition of interfering molecules, a further addition of 2 mM glucose resulted in a significant increase in the current density indicating negligible influence of interfering molecules on electrocatalytic activity of Ni-BT/Au electrode towards glucose oxidation. The electrochemical response of Ni-alkanethiolate films/ Au mesh electrode towards glucose is comparable to the state-of-the-art results in literature (Table 1.1).[Karikalan et al., 2016; Yang et al., 2016]

The bar graph representing variation in current ratio response with the respective electrodes is shown in Figure 3.17a. The fluctuation in the current response for glucose detection was found to lie within the limit (<5%) for all the respective electrodes giving an excellent reproducibility of results. The Ni-BT/Au mesh electrodes are found to be stable easily over hundreds of cycles (Figure 3.17b).

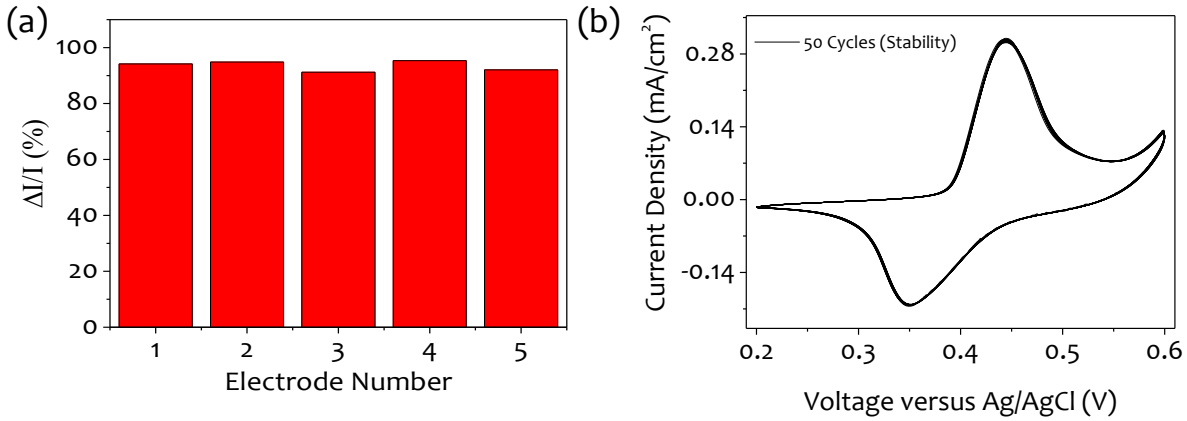

Figure 3.17: (a) Bar graph representing the changes in current ratio (ΔI/I) % with respect to the electrode derived from CV measurements with and without glucose. (b) Consecutive cyclic voltammetry measurements at 50 mV/s for stability test.

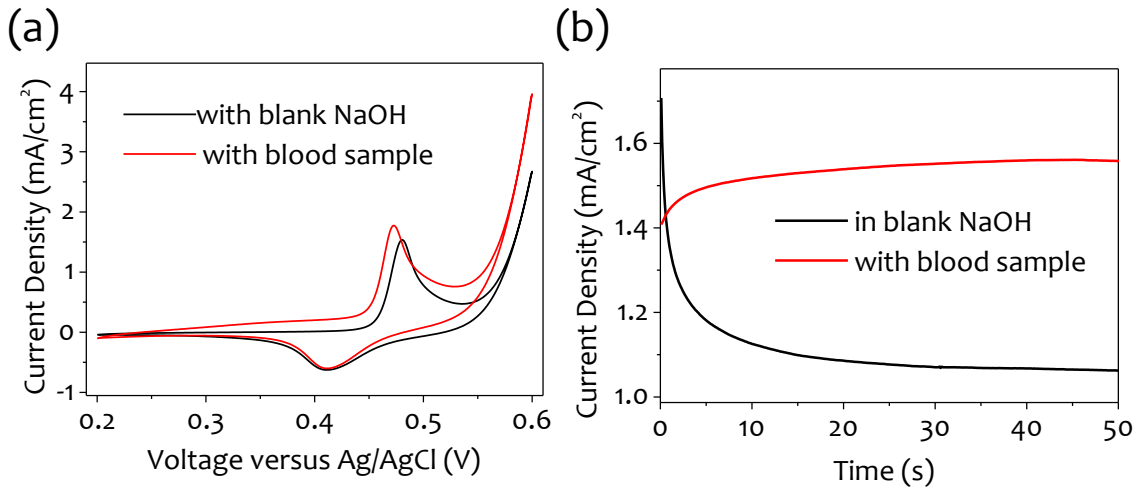

Figure 3.18: (a) CV measurements and (b) I-t measurements before and after addition of real blood sample to t 0.1 M NaOH electrolyte.

To evaluate the real time application, we further tested the Ni-BT/Au mesh electrode with diluted blood sample. The 5 µL of blood sample was taken from a diabetic patient as volunteer and the initial blood glucose was measured with commercially available glucose sensor (Accu Check) and the blood glucose was estimated to be around 0.85 mM. The 5 µL of blood was diluted 20 times in 0.1 M NaOH to prepare the sample for measurement. CV measurement was carried out in 10 mL of blank 0.1 M NaOH and with the addition of 1 mL of diluted blood solution to 10 mL of NaOH, the peak current increased significantly as shown in Figure 3.18a. I-t measurement carried out 0.6 V for the blank sample and the blood sample containing electrolyte exhibited a clear increase in current indicating the sensitivity of sensor towards low volume of glucose present (Figure 3.18b). A separate calibration curve is required

to correctly estimate the value however this is only meant to realize the working of the sensor. Further, clinical tests and optimization will be required to establish the glucose sensor developed in this study for practical application.

3.5 Conclusions

In summary, we have demonstrated a simple method for fabrication of thin film electrode by using Ni alkanethiolates as single source precursor. This method, unlike conventional methods, involves simple drop coating of precursor ink on Au electrode followed by its electro-oxidation instead of any heating processes or use of any binders and additives. These unique features of electrode fabrication make it an easily scalable manufacturing process. Different chain lengths of thiolate inks were prepared for electrode fabrication. Ni-BT ink was found to have a lower potential (0.55 V) and high current density (1.06 mA/cm^2) for redox activity which makes it a good material for enhanced electrocatalytic applications. The fabricated electrodes were used for non-enzymatic glucose sensing. The transparent Ni-BT/Au mesh has a wide range of glucose concentration of 0.5 - 2 mM in the lower region and 2 - 11 mM for the higher region and is, in fact, better than Ni-BT/FTO electrode. The transparent Ni-BT/Au mesh electrodes had a large number of accessible sites for rapid electron transfer and synergetic effects of Au mesh and Ni-BT due to the larger projection area enable Au mesh based glucose sensor to exhibit a wide linear range and lower LOD. One can use such electrodes conveniently as a one-time chip for sensing of glucose in blood serum and bodily fluids such as urine and tears, present in low concentrations. In future, these transparent electrodes can be extended to optical based dual detection in combination with electrochemical measurement for robustness and accurate result.